O_2-Assisted Methane Oxidation on Single-Atom Pd@SSZ-13: A Combined First-Principles and Microkinetic Study

Anuroopa Behatha,[†] Shalini Tomar,[†] Hojin Jeong,[‡] Joon Hwan Choi,[*,‡] Seung-Cheol Lee,[*,†,¶] and Satadeep Bhattacharjee[*,†]

†*Indo-Korea Science and Technology Center (IKST), Bangalore 560064, India*

‡*Functional Ceramics Department Korea Institute of Materials Science (KIMS) 797 Changwon-daero, Seongsan-gu, Chanwon-si, Gyeongsangnam-do, 51508, South Korea*

¶*Electronic Materials Research Center, Korea Institute of Science & Technology, Seoul 130-650, Korea*

E-mail: jchoi@kims.re.kr; leesc@kist.re.kr; s.bhattacharjee@ikst.res.in

Framework Structure of SSZ-13 Zeolite

Figure S1 illustrates the detailed depiction of the SSZ-13 zeolite framework, emphasizing its characteristic 6-,4-,8-MR rings motifs. Panel (a) displays the six-membered and four-membered rings (6MR and 4MR), while panel (b) displays the eight-membered (8MR) ring channels. The insets highlight the respective pore windows, with the maximum Si–Si distances measured to be 6.28 Å for the 6MR, 4.41 Å for the 4MR, and 8.06 Å for the 8MR.

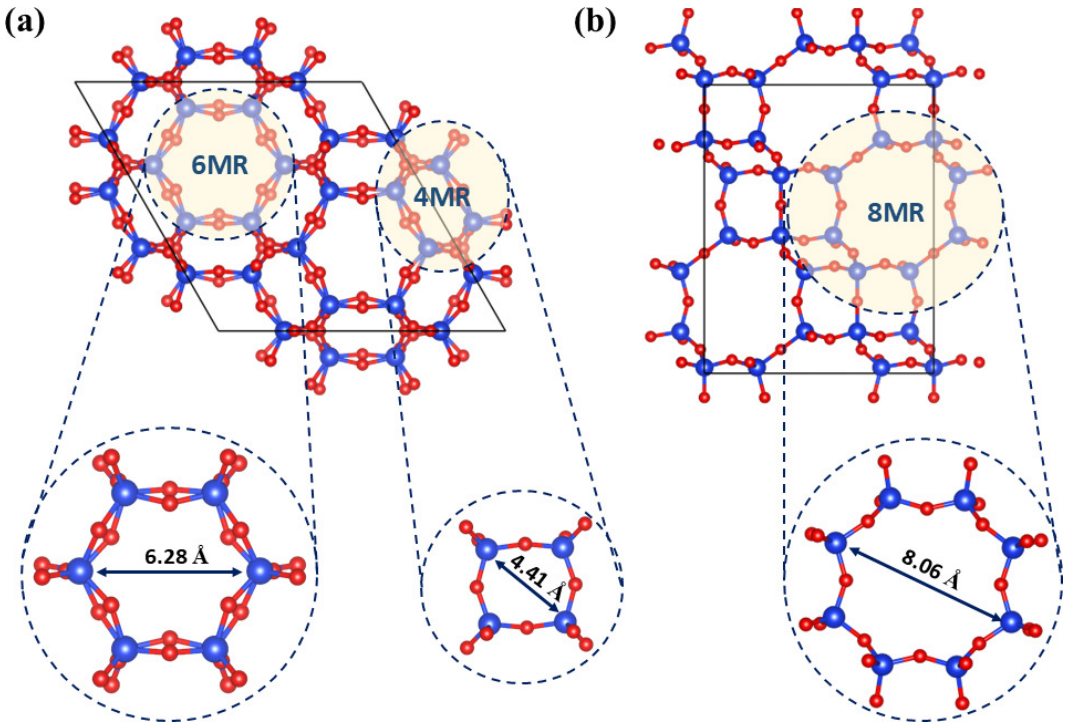

Figure S1: (Color online) Detailed representation of the SSZ-13 zeolite framework highlighting its 6-, 4- and 8-membered ring structures. Insets show the corresponding pore openings with maximum Si-Si separations of 6.28 Å (6MR), 4.41 Å (4MR) and 8.06 Å (8MR). Here, red and blue atoms represents O and Si atoms respectively.

Model construction for Pd active site recognition

The catalytic models employed in this work were constructed starting from the fully periodic bulk SSZ-13 (CHA-type) zeolite framework. The pristine SSZ-13 structure consists of interconnected cages formed by 4-, 6-, and 8-membered rings (MRs), as illustrated in Fig. S2. All calculations were performed using the optimized bulk unit cell, and no slab or surface cleavage was introduced at any stage. Al substitution was introduced by replacing two framework Si atoms with Al, resulting in an Al-substituted SSZ-13 framework while preserving the overall periodicity of the zeolite lattice [Fig. S2]. The Al substitution creates negatively charged framework oxygen atoms, which define chemically relevant anchoring sites for metal incorporation within the internal pore environment. The catalytic "pore surface" considered in this study therefore corresponds to the internal pore walls of the three-dimensional zeolite framework rather than an external surface. Pd incorporation was modeled by placing

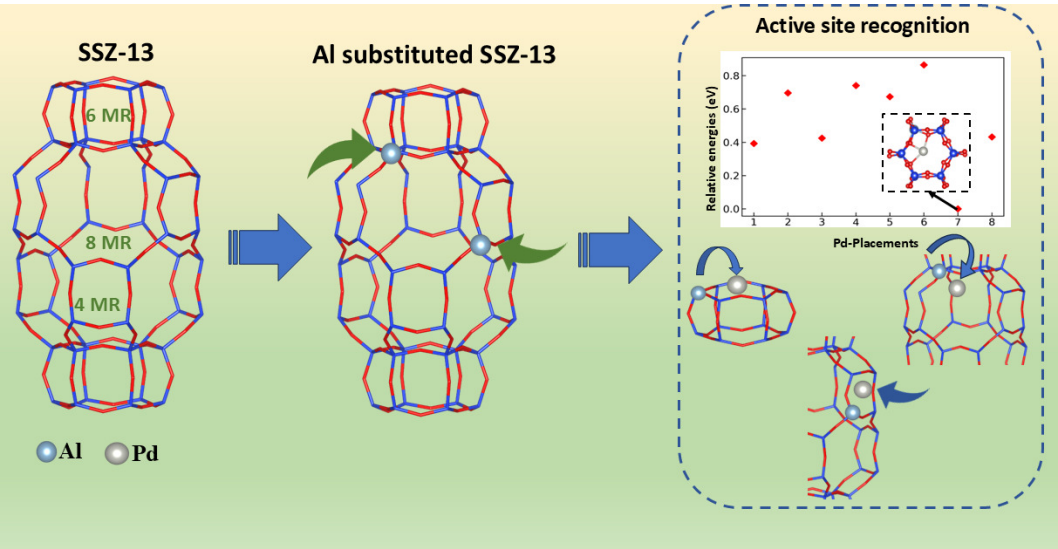

Figure S2: (Color online) Schematic illustration of the model construction and Pd active-site identification procedure highlighting the Pristine SSZ-13 framework with 4-, 6-, 8- MR environments (left), Al-substitution in SSZ-13 framework (middle) and Active site recognition steps of Pd over Al-substituted SSZ-13.

a single Pd atom at several chemically reasonable initial positions within the zeolite pore, primarily in the vicinity of Al-associated framework oxygen atoms and near different ring environments (4-, 6-, and 8-membered rings). These trial configurations were chosen to sample distinct local coordination environments accessible within the pore space. Each Pd placement was subsequently fully relaxed using density functional theory until all residual forces were below the chosen convergence threshold. To identify the most stable catalytic configuration, the total energies of the relaxed Pd-containing structures were compared. The relative energies of the different Pd placements are summarized in Fig. S2, where energies are referenced to the lowest-energy configuration. The most stable Pd site corresponds to a Pd atom coordinated to framework oxygen atoms adjacent to Al within the 6-membered ring region of the CHA cage. This configuration was selected as the representative active site for all subsequent adsorption, reaction pathway, and microkinetic modeling calculations.

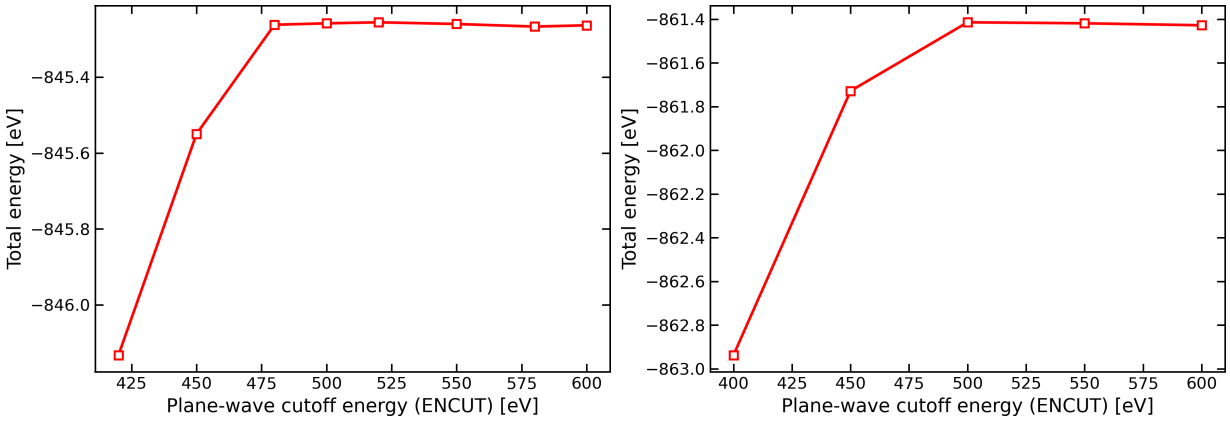

Figure S3: (Color online) Convergence of the total energy as a function of the plane-wave cutoff energy (ENCUT) for (a) Al-substituted SSZ-13 framework (b) the Pd adsorbed Al-substituted SSZ-13.

Convergence tests

Convergence tests has been first performed for the Al-substituted SSZ-13 framework, which serves as the base system for all subsequent calculations. The plane-wave cutoff energy used for all calculations was set to 500 eV, and its adequacy was validated through explicit convergence tests as shown in Fig. S3(a). In addition, this convergence behavior has been verified for the representative Pd-adsorbed configurations with the Al-substituted SSZ-13 framework. No meaningful changes in the energy trend were observed upon Pd-adsorption (see Fig.S3(b)). The total energy variation beyond this cutoff is on the order of 5 meV, indicating that the chosen ENCUT is sufficient for a reliable description of the electronic wave functions and charge density. The k-point sampling was also systematically tested for Al-substituted SSZ-13 framework. As shown in Fig. S4, total energies obtained using 1×1×1 (Γ-point), 2×2×2, 3×3×2, and 3×3×3 k-point meshes differ by less than 2 meV, confirming that Γ-point sampling is sufficient for the large insulating zeolite unit cell considered here. All subsequent geometry optimizations and reaction energy calculations were therefore performed using Γ-point sampling.

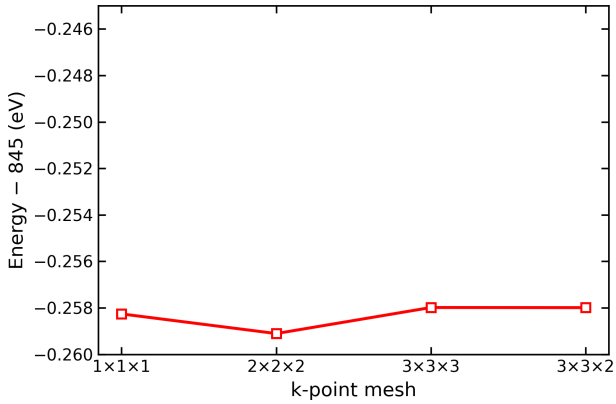

Figure S4: (Color online) K-point convergence test performed for Al-substituted SSZ-13 framework. Energies are plotted relative to -845 eV for clarity.

NEB vs Semi emphirical relations

Figure S5 illustrates the correlation plot of estimated activation barriers using semi-empirical relations (BEP and UBI-QEP) with CI-NEB. Both the approaches provide reliable estimates of the NEB-derived activation barriers for successive C-H bond scissions in methane. As seen in Fig. S5a, the standard interpolation parameter in UBI-QEP (i.e $\phi = 0.50$) systematically underestimates the barriers (MAE 0.33 eV, R^2=0.56), whereas tuning to $\phi = 0.81$ (or $\phi = 0.85$) collapses that bias and yields near-quantitative agreement (MAE 0.10-0.13, R^2 0.92-0.94). Likewise, a family of BEP fits shows progressive improvement as the slopes are adjusted ($\Gamma = 0.93 \rightarrow 0.77$) with best-performing parametrizations giving MAE 0.10-0.11 and R^2 0.94-0.95. Overall, we can notice that the scaling relations, when carefully calibrated, can capture the essential energetics of methane activation on Pd/SSZ-13 with near-quantitative accuracy.

TOF

The turnover frequency (TOF) profiles show a strong dependence on temperature, while the influence of pressure remains relatively minor. Figure S6 shows that CH_4 dissociation becomes significant around 700–800 K, especially at higher pressures, while CH_3, CH_2, and

CH dissociation occur only at much higher temperatures ($\geq$ 900 K). Pressure promotes CH_4 activation by shifting activity to lower temperatures, but its effect on later C–H cleavages is minimal, indicating that methane activation starts with CH_4 breaking, while subsequent steps are kinetically harder.

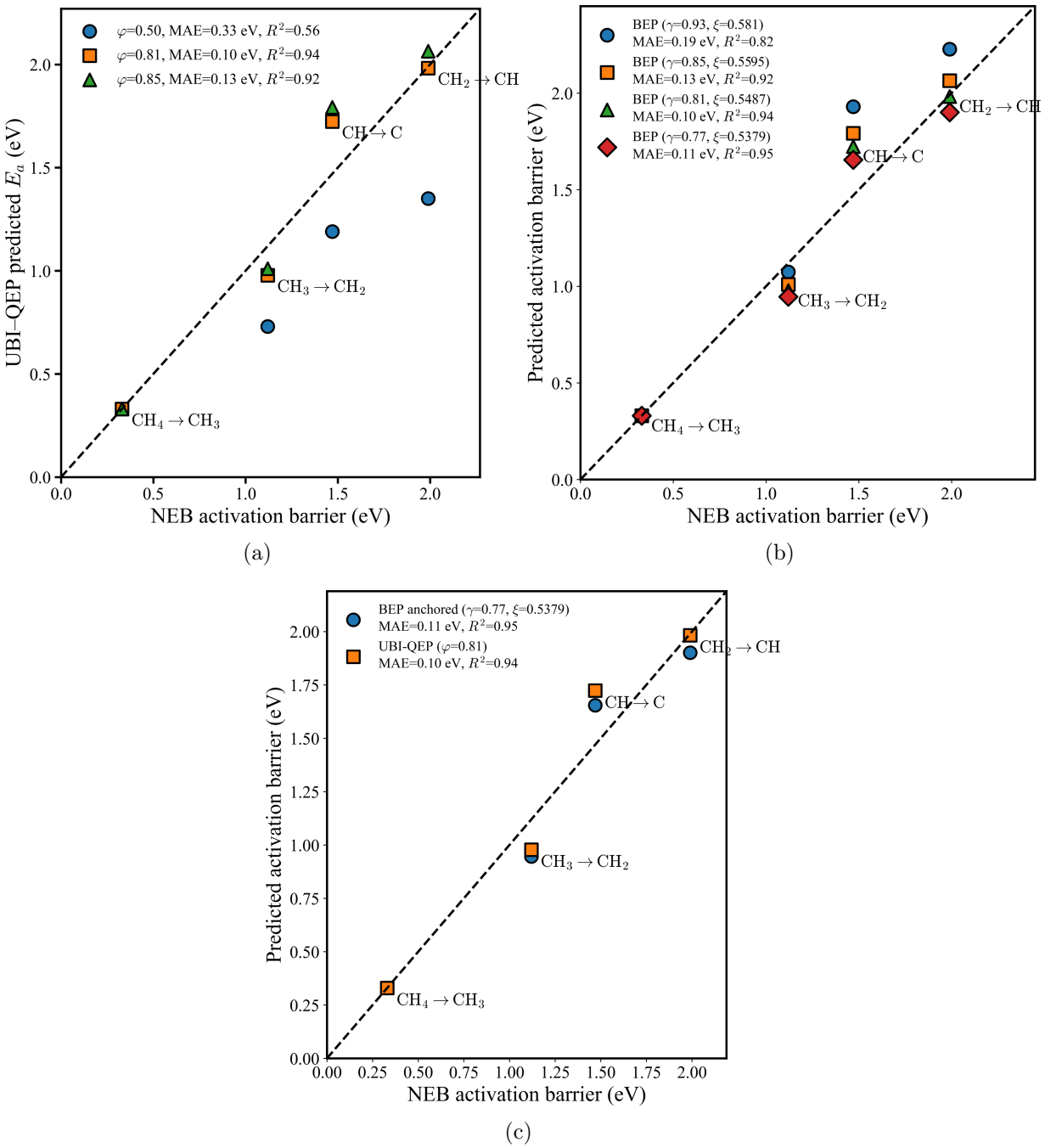

Figure S5: (Color online) (a) Effect of interpolation parameter (ϕ) inthe UBI-QEP model on the agreement with NEB activation barriers. (b) Performance of BEP relations with varying slope in reproducing NEB barriers for methane C-H bond scission.(c) Comparision between NEB-calculated activation barriers and the predictions from anchored BEP and UBI-QEP approaches.

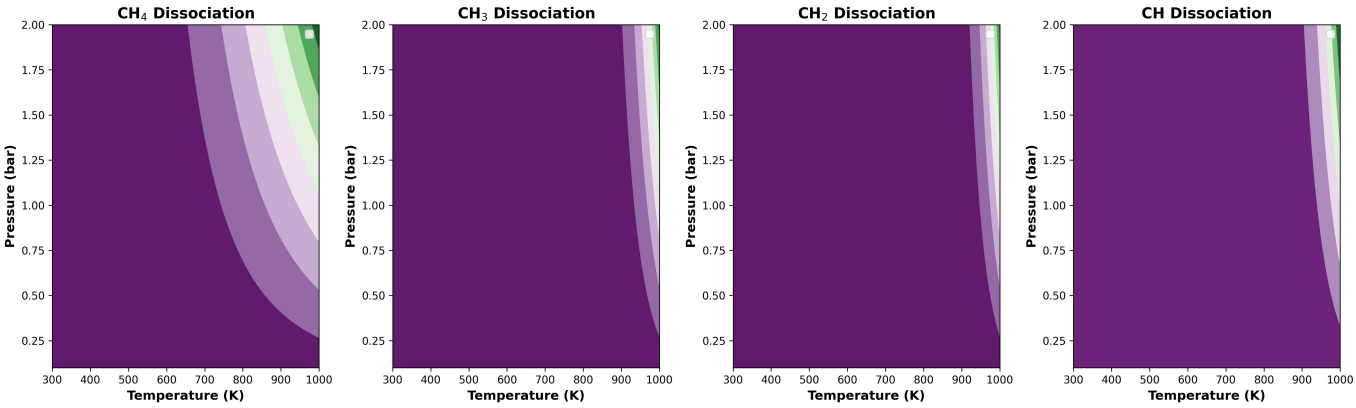

Figure S6: The turnover frequency (in s^{-1}) of CH_4, CH_3, CH_2 and CH dissociation concerning temperature (in K) and pressure (in bar).